THE JOURNAL OF BIOLOGICAL CHEMISTRY
Vol. 279, No. 8, Issue of February 20, pp. 6815–6823, 2004
Printed in U.S.A.

A Substrate-induced Switch in the Reaction Mechanism of a Thermophilic Esterase

KINETIC EVIDENCES AND STRUCTURAL BASIS*

Received for publication, July 17, 2003, and in revised form, November 13, 2003
Published, JBC Papers in Press, November 15, 2003, DOI 10.1074/jbc.M307738200

Giuseppina De Simone‡§, Luigi Mandrich§¶‖, Valeria Menchise‡, Valeria Giordano‡, Ferdinando Febbraio¶, Mosè Rossi¶, Carlo Pedone‡, and Giuseppe Manco¶‡‡**

From the ‡Istituto di Biostrutture e Bioimmagini-Consiglio Nazionale delle Ricerche, via Mezzocannone 6, 80134 Naples, Italy and the ¶Istituto di Biochimica delle Proteine-Consiglio Nazionale delle Ricerche, Via P. Castellino 111, 80131 Naples, Italy

The reaction mechanism of the esterase 2 (EST2) from *Alicyclobacillus acidocaldarius* was studied at the kinetic and structural level to shed light on the mechanism of activity and substrate specificity increase previously observed in its double mutant M211S/R215L. In particular, the values of kinetic constants (k_1, k_{-1}, k_2, and k_3) along with activation energies (E_1, E_{-1}, E_2, and E_3) were measured for wild type and mutant enzyme. The previously suggested substrate-induced switch in the reaction mechanism from $k_{cat} = k_3$ with a short acyl chain substrate (*p*-nitrophenyl hexanoate) to $k_{cat} = k_2$ with a long acyl chain substrate (*p*-nitrophenyl dodecanoate) was validated. The inhibition afforded by an irreversible inhibitor (1-hexadecanesulfonyl chloride), structurally related to *p*-nitrophenyl dodecanoate, was studied by kinetic analysis. Moreover the three-dimensional structure of the double mutant bound to this inhibitor was determined, providing essential information on the enzyme mechanism. In fact, structural analysis explained the observed substrate-induced switch because of an inversion in the binding mode of the long acyl chain derivatives with respect to the acyl- and alcohol-binding sites.

Esterase 2 (EST2)[1] from the thermophilic eubacterium *Alicyclobacillus acidocaldarius* is a thermostable serine hydrolase belonging to the hormone-sensitive lipase family of the esterase/lipase superfamily (1–3). Members of this family are ubiquitous (see the ESTHER database), comprise true lipases and amidases other than carboxylesterases, and are still poorly characterized. For some of them a role in lipid catabolism or detoxification has been proposed (4, 5).

EST2 hydrolyzes monoacyl esters of different acyl chain length, triglycerides of short acyl chain, and different compounds of pharmacological and industrial interest (3, 6). The *est2* gene has been overexpressed in *Escherichia coli*, and the protein, a monomeric B-type carboxylesterase of about 34 kDa, was purified and characterized. The enzyme displays an optimal temperature at 70 °C and maximal activity with *p*-nitrophenyl (*p*NP) esters having an acyl chain of six to eight carbon atoms (3). Biochemical and mutagenic studies have allowed the identification of residues of the catalytic triad and oxyanion hole (7).

The EST2 crystal structure was recently solved by our group as a covalently bound Hepes adduct (8), thus making it possible to obtain an unambiguous view of the active site and to detect the binding pockets for the acyl and alcohol chains of the ester substrate. On the basis of these structural data, EST2 variants with preferential specificity toward monoacyl esters with acyl chain length greater than eight carbon atoms were designed and generated by site-directed and saturation mutagenesis (9). M211S and R215L mutants and M211S/R215L double mutant were obtained, all having the desired properties in a mixed propan-2-ol/water medium (9). In particular, a 6-fold increase of the specificity constant of the double mutant for *p*NP-dodecanoate was observed; this effect was ascribed to a parallel increase in substrate affinity (decreased K_m) and catalytic activity (increased k_{cat}). Interestingly no changes in the temperature optimum and thermostability were measured for these mutants (9). In addition, preliminary kinetic results suggested a surprising inversion of the reaction mechanism, depending on the length of the ester acyl chain.

With the aim to better characterize the reaction mechanism of these enzymes and to give an explanation of the observed activation effect, these properties were further analyzed both at the kinetic and structural level. The three-dimensional structure of double mutant complexed with a long acyl chain sulfonyl derivative was solved providing a structural explanation of the enzyme kinetic behavior.

EXPERIMENTAL PROCEDURES

Materials—All chemicals were reagent grade. *p*NP-dodecanoate, *p*-nitrophenyl dodecyl ether, and 1-hexadecanesulfonyl chloride were purchased from Sigma.

Overexpression and Purification of Enzymes—Wild type and double mutant constructs were used for cell transformation and protein overexpression as reported previously (9). Purification of the recombinant enzymes was performed as described previously for the wild type (3, 9). The purified proteins were stored at 4 °C in 25 mM Tris/HCl, pH 8.3, 2.5 mM $MgCl_2$, 0.5 mM EDTA.

Covalent Binding of 1-Hexadecanesulfonyl Chloride—1-Hexadecanesulfonyl chloride (HDSC) dissolved in pure ethanol was incubated over-

* This work was supported in part by grants from the National Research Council of Italy (CNR) Target Project "PF-Biotechnology" and from the Regione Campania Legge 41/94 Year 2000. The costs of publication of this article were defrayed in part by the payment of page charges. This article must therefore be hereby marked "*advertisement*" in accordance with 18 U.S.C. Section 1734 solely to indicate this fact.

The atomic coordinates and structure factors (code 1QZ3) have been deposited in the Protein Data Bank, Research Collaboratory for Structural Bioinformatics, Rutgers University, New Brunswick, NJ (http://www.rcsb.org/).

§ Both authors contributed equally to this work.

‖ Supported by a Ph.D. grant from the University Federico II of Naples.

** To whom correspondence may be addressed. Tel.: 39-081-2536651; Fax: 39-081-5514305; E-mail: pedone@chemistry.unina.it.

‡‡ To whom correspondence may be addressed. Tel.: 39-081-6132296; Fax: 39-081-6132248; E-mail: g.manco@ibp.cnr.it.

[1] The abbreviations used are: EST2, esterase 2; *p*NP, *para*-nitrophenyl; HDSC, 1-hexadecanesulfonyl chloride.

night at 4 °C with M211S/R215L in a molar ratio of 3:1. After incubation the protein sample was loaded onto a gel filtration column (Sephadex G-25, Sigma) to eliminate the unreacted inhibitor. The covalent adduct of HDSC with the enzyme was assayed to verify the complete loss of esterase activity. Thereafter the purified complex was concentrated to 4 mg ml^{-1} and crystallized at 22 °C.

Enzyme Assays—The time course of the esterase-catalyzed hydrolysis of *p*NP-dodecanoate was followed by monitoring *p*-nitrophenoxid production at 405 nm in 1-cm path length cell with a CARY 100 Scan spectrophotometer (Varian). Initial rates were calculated by linear least-squares analysis of time courses comprising less than 10% of the total turnover.

Esterase assays were performed at 70 °C in 40 mM Na_2HPO_4/NaH_2PO_4 buffer, pH 7.1, containing 4% (v/v) acetonitrile and *p*NP-dodecanoate at different concentrations. A stock solution of *p*NP-dodecanoate was prepared by dissolving substrate in pure acetonitrile.

Kinetic Measurements and Analysis—Initial velocity *versus* substrate concentration data were fitted to the Lineweaver-Burk transformation of the Michaelis-Menten equation by weighted linear least-squares analysis with a personal computer and the GRAFIT program (10). Assays were done in duplicate or triplicate, and values for kinetic data were the mean of two independent experiments.

Steady-state rate constants in Scheme 1 are related to the experimental values of K_m and k_{cat} by the following equations.

$$k_{cat} = k_2k_3/k_2 + k_3 \quad \text{(Eq. 1)}$$

$$s = k_{cat}/K_M = k_1k_2/k_{-1} + k_2 \quad \text{(Eq. 2)}$$

$$K_m = k_3(k_{-1} + k_2)/k_1(k_2 + k_3) \quad \text{(Eq. 3)}$$

In this system there are four independent rate constants (k_1, k_{-1}, k_2, and k_3) that define two independent Michaelis-Menten parameters (K_m and s), and thus it is not possible, from experimental measurements, to resolve the individual steps of the catalytic mechanism (Scheme 1). For this reason we used a method introduced by Di Cera and co-workers (11) to determine the individual rate constants in the kinetic mechanism. The method exploits the temperature dependence of s and k_{cat} in Equations 1 and 2. The temperature dependence of a rate constant obeys the Arrhenius low,

$$k = k_0\exp\{-E/R(1/T - 1/T_0)\} \quad \text{(Eq. 4)}$$

where E is the activation energy associated with the rate constant k, R is the gas constant, T is the absolute temperature, and k_0 is the value of k at the reference temperature T_0 = 298.16 K. Substitution into Equations 1 and 2 make it possible to relate the measurement of s and k_{cat} as a function of temperature to the rate constants and related activation energies (11). Resolution of the system, and opportunely made simplifying assumptions (see Ref. 11 and "Results"), allowed the calculation of all parameters.

Determination of K_i and k_i for 1-Hexadecanesulfonyl Chloride by Time-dependent Inactivation—HDSC was dissolved in ethanol at a concentration of 5 mM and subsequently diluted to 1 mM in 40 mM sodium phosphate, pH 7.1.

Samples of EST2 or M211S/R215L double mutant (final concentrations, ~90 μg/ml) in 40 mM sodium phosphate, pH 7.1, were incubated in the presence of several concentrations of HDSC. At each time interval, aliquots were removed from the inactivation mixture, opportunely diluted in 40 mM sodium phosphate, pH 7.1, and immediately assayed in 1 ml of 160 μM *p*-nitrophenyl caproate in 40 mM sodium phosphate, pH 7.1, 4% (v/v) acetonitrile at 30 °C.

The rate constant at each inactivator concentration, k_{obs}, was determined by plotting the logarithm of the fraction of remaining active enzyme against time. K_i, the dissociation constant, and k_i, the rate constant for inactivation, were calculated by a non-linear regression fit (GRAFIT program, Ref. 10) of the observed rate constants to the following expression.

$$k_{obs} = \frac{k_i[I]}{K_i + [I]} \quad \text{(Eq. 5)}$$

Binding Studies—The affinity of *p*NP-dodecyl ether was measured by following the variation of intrinsic fluorescence of the M211S/R215L mutant enzyme upon ether binding. All fluorescence measurements were performed in 20 mM phosphate buffer and 4% (v/v) acetonitrile at 25 °C on a Jasco FP 777 spectrofluorometer. Aliquots of the inhibitor were added to the enzyme solution (0.015 mg ml^{-1}), and fluorescence was measured at 339 nm with excitation at 295 nm. After appropriate corrections for buffer and dilution, experimental binding points were fitted to a hyperbolic curve by the GRAFIT program (10). The stock solution of *p*NP-dodecyl ether was prepared in pure acetonitrile.

TABLE I
Kinetic parameters of EST2 wild type and variants (9) on pNP-dodecanoate as substrate dissolved in acetonitrile 4% (v/v)

Data reported were the mean of at least two experiments. The S.E. was not higher than 5%. Assays were performed at pH 7.1. wt, wild type.

Enzyme	k_{cat}	K_m	k_{cat}/K_m
	s^{-1}	μM^{-1}	$\mu M^{-1}\ s^{-1}$
EST2 wt	340 ± 4	4.3 ± 0.6	78 ± 8
M211S	350 ± 3	2.4 ± 0.3	146 ± 10
R215L	705 ± 3	4.6 ± 0.3	153 ± 9
M211S/R215L	940 ± 5	3.4 ± 0.5	276 ± 12

Crystallization and X-ray Data Collection—Crystals of M211S/R215L-HDSC complex were grown using the hanging drop vapor diffusion method setting up 2 μl of complex solution mixed with 2 μl of reservoir solution consisting of 2 M ammonium sulfate, 0.1 M Tris buffer (pH 8.5). Crystals of 0.1 × 0.2 × 0.2 mm^3 were grown in 2 weeks. Crystals belong to the space group $P4_12_12$ with unit cell dimensions a = b = 85.19 Å and c = 103.58 Å with one complex per asymmetric unit.

A complete data set was collected at 2.3-Å resolution from a single crystal, flash cooled at 100 K from precipitant solution containing 10% (v/v) glycerol, on a MAR Research image plate system at the European Molecular Biology Laboratory beam line X13 at Deutsches Elektronen Synchrotron, Hamburg, Germany.

Diffracted intensities were processed using the HKL crystallographic data reduction package (12). Data processing statistics are given in Table IV.

Structure Determination and Refinement—The structure of the M211S/R215L-HDSC complex was solved by molecular replacement (13). The x-ray structure of the carboxylesterase (EST2) from *A. acidocaldarius* (Protein Data Bank code 1EVQ) (8) was used as the molecular replacement search model. The rotation and translation functions were calculated using data between 15.0- and 3.5-Å resolutions. The one body translation search, using centered-overlap function, on the first 50 rotation solutions led to a single solution with a correlation coefficient of 60.9 and an R-factor of 0.388.

The electron density maps calculated at this stage of the refinement showed prominent electron density features in the active site region. After an initial refinement, limited to the enzyme structure (R-factor, 0.233; R_{free}, 0.267), a model for the HDSC covalently bound to Ser^{155} was easily built and introduced into the atomic coordinates set for further refinement, which proceeded to convergence with continuous map inspection and model updates. The refinement was carried out with the program CNS (14), while model building and map inspections were performed using the program O (15). The final crystallographic R-factor and R_{free} values calculated for the 16,467 observed reflections (in the 20.00–2.30-Å resolution range) were 0.174 and 0.216, respectively. The statistics for refinement are summarized in Table IV. Coordinates and structure factors have been deposited with the Protein Data Bank (accession code 1QZ3).

Molecular Modeling—All calculations and graphical analyses were run on a Silicon Graphics workstation. The INSIGHT/DISCOVER program (Biosym Technologies) was used to perform energy minimization at pH 7.0 using the CVVF force field. In all simulations, Arg and Lys side chains were positively charged, whereas Glu and Asp side chains were negatively charged. Energy minimization was carried out using the conjugate gradient algorithm. These procedures were stopped when the maximum derivative was 0.01 kcal/mol.

RESULTS

Substrate-induced Switch of Catalytic Mechanism

In a previous study, kinetic constants for wild type EST2 and mutant M211S/R215L were measured in the presence of propan-2-ol, which was demonstrated to be a competitive inhibitor for the enzyme (9). Since propan-2-ol could work as a nucleophile stronger than water, thus interfering with the reaction mechanism and complicating the interpretation of kinetic results, we first remeasured the kinetic parameters of these enzymes in the presence of acetonitrile as reported in Table I. The analysis of the specificity constants showed a 4-fold in-

$$E+S \underset{k_{-1}}{\overset{k_1}{\Leftrightarrow}} ES \xrightarrow{k_2} EP+R\text{-}OH \xrightarrow{k_3} E+P$$

SCHEME 1

crease for M211S/R215L and a 2-fold increase for M211S or R215L with respect to wild type. These data confirmed the results obtained previously (9).

The general mechanism of an esterase reaction is shown in Scheme 1. One simple way to get an idea about the reaction mechanism is to measure the *p*NP "burst," which is supposed to occur when the enzyme is added to the reaction mixture before the onset of the catalytic reaction, provided the release of the acid/ester is slow compared with the release of the alcohol. In Fig. 1 we report the same experiment performed for wild type EST2 and double mutant with the best substrate for wild type, namely *p*NP-hexanoate, and with the best substrate for double mutant, namely *p*NP-dodecanoate. In the case *p*NP-hexanoate, immediate release of *p*NP increased proportionally to the concentration of both enzymes, whereas with the *p*NP-dodecanoate almost no change with the increase of enzyme concentration was observed. This suggested that, with short substrates, the rate-limiting step is the acid/ester release ($k_2 \gg k_3$ and $k_{cat} \cong k_3$). The opposite scenario was observed with substrate *p*NP-dodecanoate. In fact, the absence of a *p*NP burst with wild type and double mutant M211S/R215L indicated that the reaction mechanism was limited by the alcohol release ($k_3 \gg k_2$ and $k_{cat} \cong k_2$). Again these data confirmed our preliminary findings that a switch seems to occur in the rate-limiting step of the reaction induced by the acyl chain length of the ester substrate.

Measurement of All Individual Kinetic Constants for the EST2 Mechanism

To measure all constants (k) and activation energies (E) involved in the multistep hydrolytic reaction, the temperature dependence of kinetic constants K_m and V_{max} (Table II) was analyzed according to the methodology proposed by Ayala and Di Cera (Ref. 11 and see "Experimental Procedures"). This method does not require solvent perturbation parameters (*i.e.* viscosity changes or solvent isotope effects) that often affect the substrate-enzyme interaction. It is based on the consideration that the specificity constant s and k_{cat} are temperature-dependent entities; this dependence obeys the Arrhenius law. By measuring these constants at different temperatures it is possible to derive all the rate constants (k) associated with the single steps and the relative activation energies (E). Apart from its simplicity and accuracy, it was also interesting to ascertain the behavior of this method with a thermophilic enzyme.

As reported in Table II, K_m values for substrate *p*NP-dodecanoate were similar in the mutant with respect to the wild type; this finding was true irrespective of the temperature used for the assay. In addition, the K_m values rose steadily with increasing temperature, showing almost a doubling going from 25 to 77.5 °C. The k_{cat} values instead showed a difference of 2.5–3-fold in the overall temperature range for the mutant with respect to wild type. Data were replotted in Fig. 2, *A* and *B*, as Arrhenius plots. From the slope of these curves it was possible to calculate $k_{1,0}$, E_1, $k_{2,0}$, and E_2 by assuming that the mechanism with longer substrates is rate-limited by k_2. Unfortunately, due to technical difficulties that prevented the accurate measurement of kinetic parameters at high temperatures (such as enzyme instability in aqueous acetonitrile and high background for substrate), it was not possible to draw the plot of log s against $1/T$ over 70 °C where information on $k_{-1,0}$ and $k_{3,0}$ should be gathered (11). To obviate to this difficulty we exploited the availability of an ether analog of substrate *p*NP-dodecanoate. This compound was able to inhibit the activity of M211S/R215L at a non-saturating concentration of *p*NP-dodecanoate, whereas no inhibition was observed with non-saturating concentrations of *p*NP-hexanoate. Moreover short chain *p*NP-ethers were able to compete with *p*NP-hexanoate (data

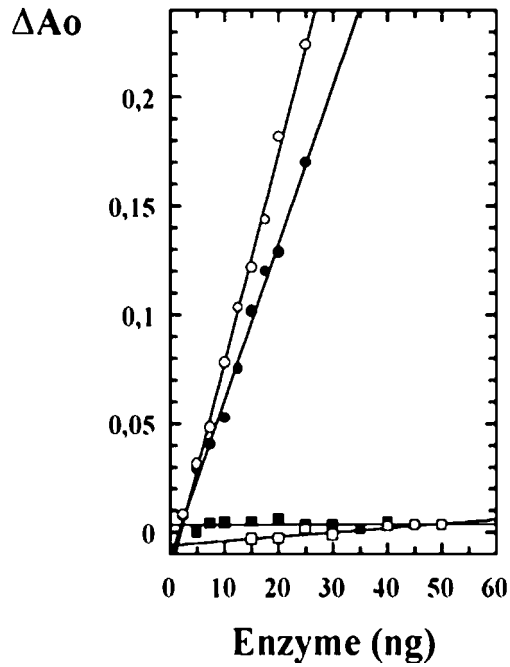

FIG. 1. **Instantaneous 'bursts' of *p*NP measured after addition of wild type or M211S/R215L enzymes to the assay mixtures.** Shown are the readings at 405 nm and at zero time of assay mixtures containing *p*NP-hexanoate (C_6) or *p*NP-dodecanoate (C_{12}) after the addition of the indicated amounts of wild type (*empty circles* for C_6 and *empty squares* for C_{12}) or M211S/R215L (*filled circles* for C_6 and *filled squares* for C_{12}). Data were corrected for the *p*NP release due to the onset of the catalytic activity during the 4 s required to mix the enzyme with substrate and to read the absorption.

TABLE II
Temperature dependence of M211S/R215L and EST2 kinetic parameters

Assays were performed with substrate *p*-nitrophenyl dodecanoate in 40 mM phosphate buffer, pH 7.1, and 4% acetonitrile (v/v).

Temperature	Specific activity	k_{cat}	K_m	k_{cat}/K_m
°C	*units/mg*	s^{-1}	*μM*	$\mu M^{-1}\ s^{-1}$
M211S/R215L				
25	133	76	2.3 ± 0.1	33
30	178	103	2.5 ± 0.1	41
35	240	138	3.0 ± 0.2	46
45	370	212	3.1 ± 0.2	68
55	787	452	3.2 ± 0.2	141
65	1465	842	3.2 ± 0.2	270
70	1747	940	3.4 ± 0.5	276
72.5	1650	950	3.6 ± 0.4	264
75	1435	825	3.8 ± 0.4	217
77.5	1415	810	4.0 ± 0.3	203
EST2				
25	51	30	3.0 ± 0.4	10
30	63	37	2.8 ± 1.5	12
35	76	45	3.5 ± 0.15	14
45	155	85	3.9 ± 0.3	21
55	207	118	4.0 ± 0.2	29
65	340	205	4.1 ± 0.35	50
70	600	340	4.3 ± 0.6	78
72.5	580	333	4.6 ± 0.5	72
75	570	327	4.7 ± 0.3	70
77.5	580	333	4.9 ± 0.2	68

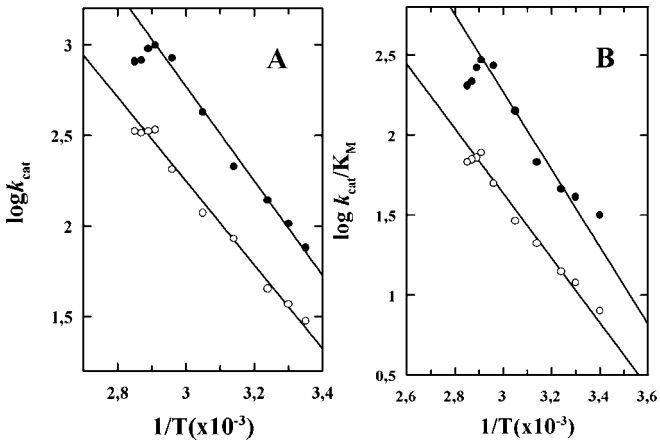

FIG. 2. **Arrhenius plots of the k_{cat} (*A*) and specificity constant $s = k_{cat}/K_m$ (*B*) for hydrolysis of *p*NP-dodecanoate by EST2 wild type (*empty circles*) and M211S/R215L (*filled circles*) variant in the temperature range from 25 to 77.5 °C.** The best fit of data points was performed with the GRAFIT program.

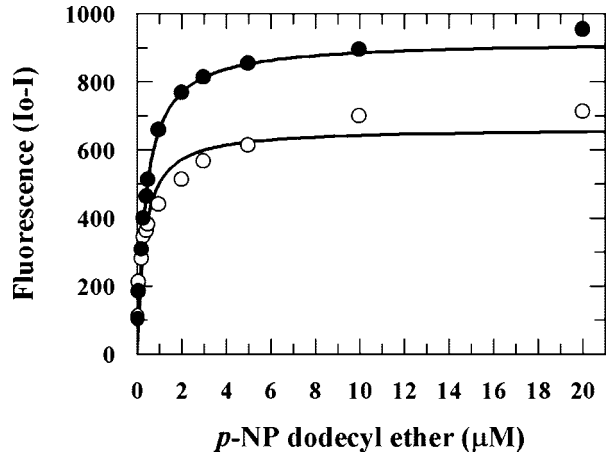

FIG. 3. **Binding curves of wild type EST2 and M211S/R215L mutant with *p*NP-dodecyl ether.** Reported is the fluorescence change of 0.015 mg ml^{-1} M211S/R215L (*empty circles*) or wild type EST2 (*filled circles*) upon binding of *p*NP-dodecyl ether at 25 °C in 20 mM phosphate buffer, pH 7.1. The *solid line* is the best fit of the data to a hyperbolic saturation curve.

not shown). We observed a dose-dependent tryptophan fluorescence increase at 339 nm when the substrate analog was added to the wild type or the M211S/R215L protein. The saturation curves (Fig. 3) allowed K_D values of 0.320 and 0.395 μmol s^{-1} for the wild type and double mutant, respectively, to be calculated. From these values, since $k_{1,0}$ was available, it was possible to calculate $k_{-1,0}$. The $k_{3,0}$ values were easily obtained from the Equation 3 of K_m (see 'Experimental Procedures') and their experimental values at 25 °C together with E_3 values from the temperature dependence of k_{cat} according to Equation 4. Finally the E_{-1} values were obtained from the temperature dependence of log *s* at high temperature (Equation 4) and from the consideration that the point at 70 °C should belong to both the curve with slope $-E_1/R$ and with slope $(E_{-1} - E_1 - E_2)/R$ (11). In Table III we report all the computed values.

TABLE III
Individual rate constants and activation energies of wild type EST2 and double mutant M211S/R215L at the reference temperature (25 °C) with pNP-dodecanoate as substrate

Parameters	EST2	M211S/R215L
$k_{1,0}$ (μM^{-1} s^{-1})	9.5 ± 0.3	31.0 ± 1.0
$k_{-1,0}$[a] (s^{-1})	3.8 ± 0.16	1.3 ± 0.1
$k_{2,0}$ (s^{-1})	27.0 ± 0.2	71.0 ± 2.0
$k_{3,0}$ (s^{-1})	334.0 ± 9.0	490.0 ± 10.0
E_1 (kcal/mol)	8.8 ± 0.6	10.2 ± 0.8
E_{-1} (kcal/mol)	18.7 ± 0.6	30.2 ± 0.9
E_2 (kcal/mol)	10.6 ± 0.5	11.7 ± 0.6
E_3 (kcal/mol)	9.2 ± 0.6	7.5 ± 0.7

[a] Estimated by measurements of K_D as described under "Experimental Procedures."

Kinetic Analysis of Inhibition with HDSC

EST2 is sensitive to the action of alkylsulfonyl chlorides (3). These inhibitors, as already observed for other lipases and esterases (16, 17), irreversibly inactivate the enzyme generating an analog of the second intermediate of the reaction pathway (Scheme 1). To start crystallographic trials with the covalently modified species, we performed a study of kinetic inactivation of double mutant with HDSC (Fig. 4). Incubation of wild type EST2 and M211S/R215L with HDSC resulted in time-dependent inactivation according to pseudo-first-order kinetics (Fig. 4, *A* and *C*). The reciprocal replot of these slopes (k_{obs}) against inhibitor concentration is shown in Fig. 4, *B* and *D*. Values for inactivation parameters for wild type EST2 (k_i = 0.013 s^{-1} and K_i = 0.35 μM) and for M211S/R215L double mutant (k_i = 0.020 s^{-1} and K_i = 0.55 μM) were obtained by a non-linear regression analysis of the data.

Crystallographic Studies

To provide a detailed structural explanation of the kinetic data measured for EST2 and its single and double mutants with long acyl chain esters, the high resolution structure of M211S/R215L complexed with HDSC was solved by x-ray diffraction studies. The protein complex was prepared and crystallized as described under "Experimental Procedures."

Quality of the Model and Overall Structure—The structure of the complex M211S/R215L-HDSC was solved by molecular replacement (AmoRe) (13) using the x-ray structure of EST2 (8) as a starting model. The complex structure was refined using the CNS program (14) to a crystallographic *R*-factor of 17.4% and an R_{free} of 21.6% in the 20.0–2.30-Å resolution range.

The final model consisted of 2431 non-hydrogen atoms, including the HDSC molecule covalently bound to the catalytic serine and 253 water molecules. Poor electron density was observed for the first two N-terminal residues. The refined structure presented a good geometry with root mean square deviations from ideal bond lengths and angles of 0.008 Å and 1.53°, respectively. The average temperature factor (B) for all atoms was 27.68 Å^2. The stereochemical quality of the model was assessed by Procheck (18). The most favored and additionally allowed regions of the Ramachandran plot contained 91.1 and 7.8%, respectively, of the non-glycine residues. The statistics for refinement are summarized in Table IV.

As expected, the three-dimensional structure of M211S/R215L within the complex was very similar to that of EST2 observed in the complex with the Hepes molecule. When superimposing all the mutant Cα atoms with those of native protein a root mean square deviation of 0.55 Å was calculated. The largest deviations were localized in the protein region Ser^{33}–Pro^{38}, which appeared disordered in EST2 and with well defined electron density maps in the complex under investigation. Focusing our attention on the protein region encompassing the two mutations, we observed that the two models superimposed well, and no structural rearrangements were found. In both structures, residues 211 and 215 were well defined in the electron density maps and constituted part of the acyl-binding pocket (8). Finally the catalytic triads displayed geometry virtually indistinguishable within the ex-

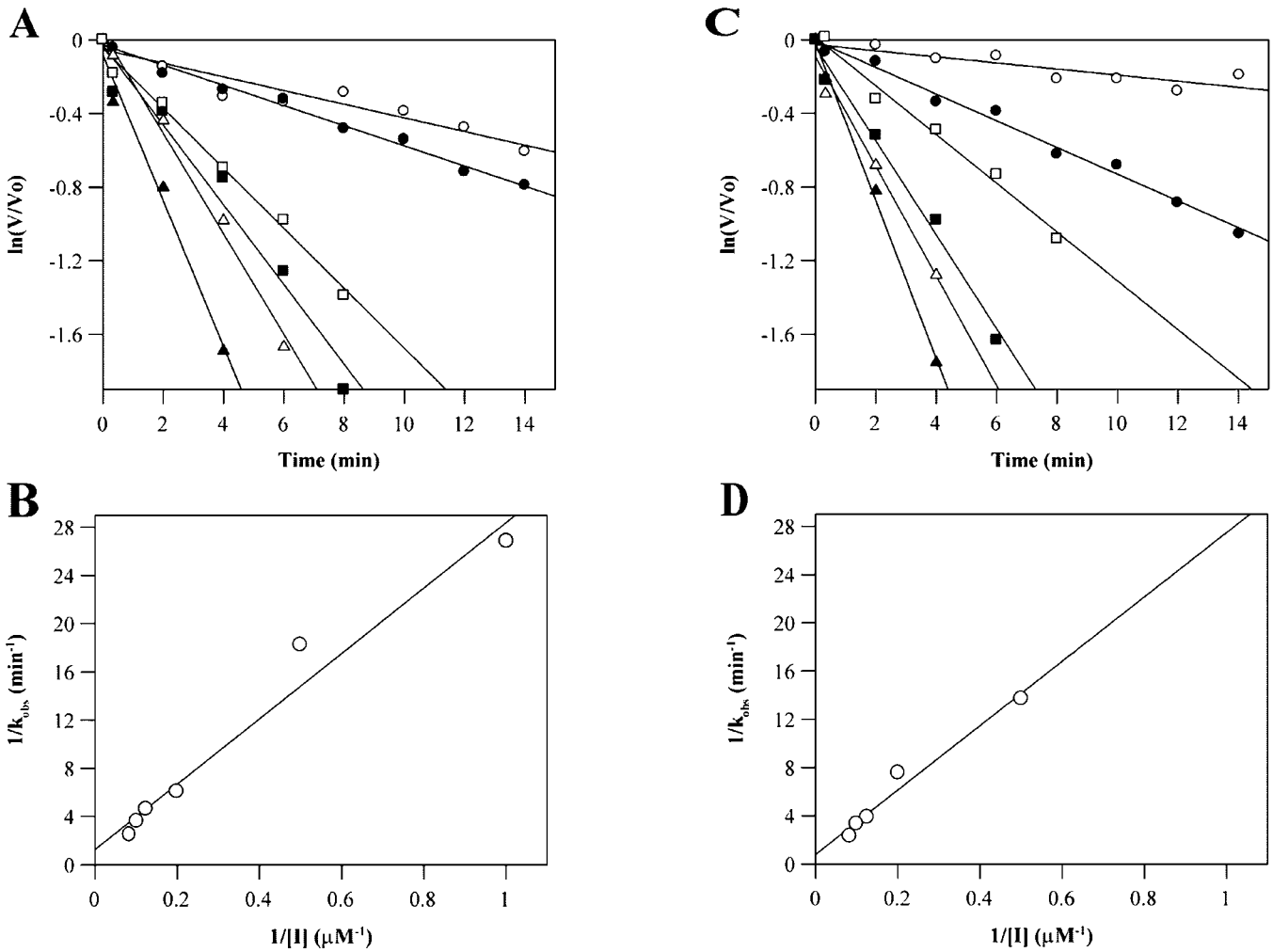

FIG. 4. **Kinetic analysis of inhibition with HDSC.** *A*, plot of logarithm of EST2 residual activity *versus* time at the following inhibitor concentrations: 1 μM (*empty circles*), 2 μM (*filled circles*), 5 μM (*empty squares*), 8 μM (*filled squares*), 10 μM (*empty triangles*), 12 μM (*filled triangles*). *B*, double reciprocal plot of first-order rate constants taken from *A versus* inhibitor concentrations. *C*, plot of the logarithm of residual activity *versus* time of M211S/R215L double mutant at the following inactivator concentrations: 1 μM (*empty circles*), 2 μM (*filled circles*), 5 μM (*empty squares*), 8 μM (*filled squares*), 10 μM (*empty triangles*), 12 μM (*filled triangles*). *D*, double reciprocal plot of first-order rate constants taken from *C versus* inactivator concentrations.

TABLE IV
Data collection and refinement statistics

Data collection statistics (20.00–2.30 Å)	
Temperature (K)	100
Total reflections	177,515
Unique reflections	17,707
Completeness (%)	
Overall	98.8
Outermost data shell	94.1
R_{sym} [a] (%)	
Overall	8.9
Outermost data shell	42.6
Mean $I/\sigma(I)$	
Overall	14.4
Outermost data shell	2.2
Refinement statistics (20.00–2.30 Å)	
R-factor[b] (%)	17.4
R_{free} [b] (%)	21.6
R.m.s.d.[c] from ideal geometry	
Bond lengths (Å)	0.008
Bond angles (°)	1.53
Number of protein atoms	2,431
Number of water molecules	253
Average B factor (Å^2)	27.68

[a] $R_{sym} = \Sigma|I_i - I|/\Sigma I_i$, overall reflections.
[b] *R*-factor = $\Sigma|F_o - F_c|/\Sigma F_o$; R_{free} calculated with 5% of data withheld from refinement.
[c] Root mean square deviation.

perimental error, thus indicating that binding of inhibitors to the active site does not affect significantly the enzyme structure.

HDSC Binding in the Active Site—Inspection of the electron density within the mutant active site, at various stages of the crystallographic refinement, demonstrated the occurrence of the bound hexadecanesulfonyl derivative (Fig. 5). The main protein-inhibitor interactions are schematically depicted in Figs. 5 and 6. According to these figures, the inhibitor, covalently bound to Ser^{155} Oγ with a tetrahedral conformation around its sulfur atom, presents a peculiar spatial arrangement with respect to the structure of the EST2-Hepes complex (8). In particular, the HDSC O-1 atom is hydrogen-bonded to the water molecule HOH41 (2.87 Å), which in turn interacts with Ser^{211} Oγ (3.04 Å), while the O-2 atom is located in the oxyanion hole being hydrogen-bonded to the NH groups of Gly^{83} (3.06 Å), Gly^{84} (2.64 Å), and Ala^{156} (2.95 Å) (Fig. 6). Quite surprisingly, the hexadecane moiety is not located in the previously identified acyl-binding pocket, which is occupied by a series of water molecules, but perfectly fits in the long and narrow hydrophobic tunnel defined by three α-helices (α1, α2, and α7), two 3_{10} helices (Ser^{35}–Leu^{36} and Phe^{284}–Phe^{287}), and the loop regions Asn^{15}–Ser^{26} and Gly^{82}–Val^{87} (Fig. 7). In previous studies, part of this tunnel was identified

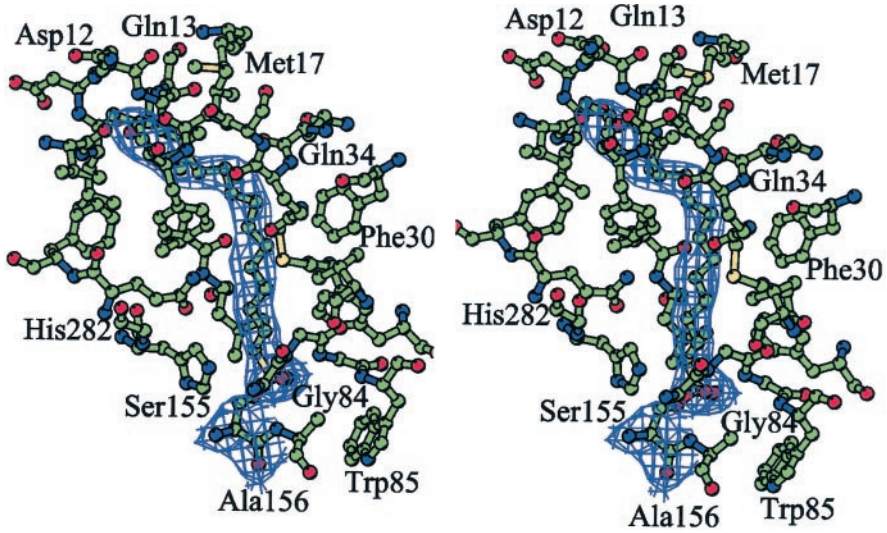

FIG. 5. **Stereoview of the active site region in the complex M211S/R215L-HDSC.** The inhibitor is shown covalently bound to the active site serine and associated with simulated annealing omit $|2F_o - F_c|$ electron density map (14) computed at 2.3 Å and contoured at 1.0 σ.

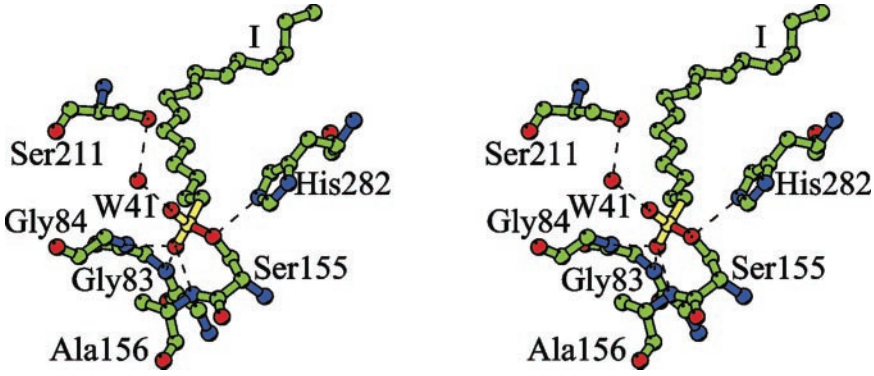

FIG. 6. **Hydrogen bond interactions between the M211S/R215L active site residues and HDSC (labeled *I*).**

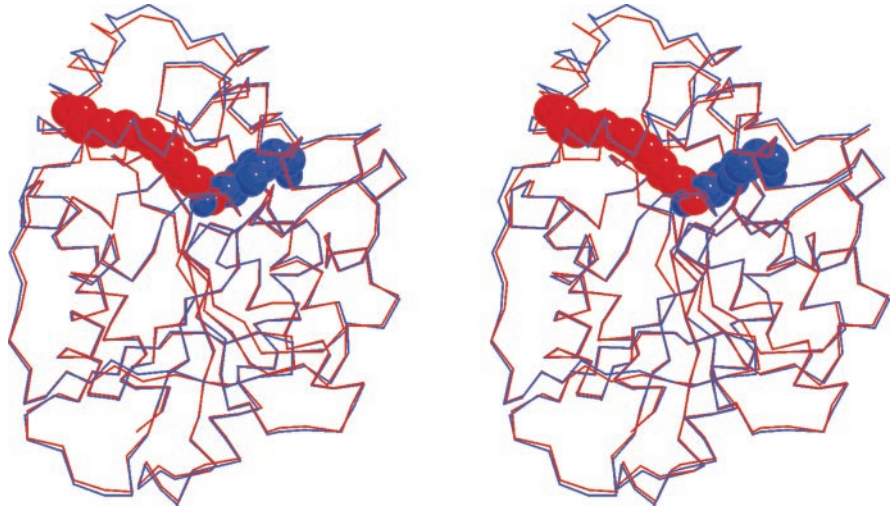

FIG. 7. **Stereoview showing the superposition of the Cα trace of EST2 (*blue*) and M211S/R215L (*red*).** HDSC and Hepes molecules are also shown. Both structures consist of a core domain, belonging to the α/β hydrolase fold family (constituted in the M211S/R215L-HDSC structure by strands β1, residues 47–55; β2, residues 58–66; β3, residues 74–80; β4, residues 107–112; β5, residues 144–154; β6, residues 179–182; β7, residues 244–249; and β8, residues 272–277, and by α-helices α3, residues 94–104; α4, residues 123–137; α5, residues 156–170; α8, residues 255–267; and α9, residues 292–309), and a cap domain (constituted in the M211S/R215L-HDSC structure by α-helices α1, residues 5–14; α2, residues 27–33; α6, residues 196–199; and α7, residues 208–218). Secondary structure assignments were obtained from Procheck (18).

as the substrate alcohol-binding pocket on the basis of structural similarity with other esterases and lipases (8). The alkyl chain of the inhibitor presents an elongated structure with most of its C–C bonds in a *trans* conformation and stabilized by numerous strong van der Waals interactions well distributed along this tunnel. It is worth noting that residues Leu[36] and Phe[37], which are involved in several van der Waals interactions with the inhibitor, in this structure are part of a short 3_{10} helix. On the contrary, these residues in EST2 are part of a flexible loop associated to poorly defined electron density maps.

A model in which the acyl-binding pocket was hypo-

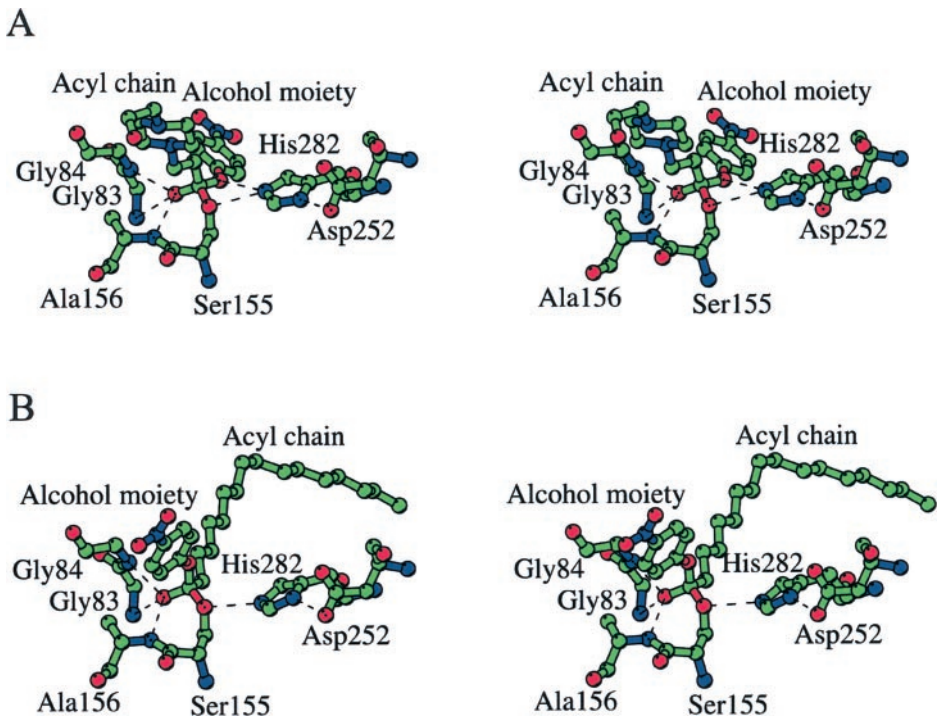

FIG. 8. **Stereoview representation of the first tetrahedral intermediate models of EST2-*p*NP-3-[4-(2-hydroxyethyl)-piperazinyl]-propionate (*A*) and M211S/R215L-*p*NP-hexadecanoate (*B*).** The inversion of the substrate orientation in the catalytic site causes a loss of the hydrogen bond between His^{282} NE-2 and the alcohol oxygen of the substrate.

thetically accommodating the hexadecane moiety was built on the basis of the structural superimposition of this enzyme with *Candida rugosa* lipase bound to an identical inhibitor (19).[2] A careful analysis of this model revealed that the inhibitor should assume an unfavorable bent conformation to perfectly fit into the acyl-binding site. This finding is strictly related to the geometrical dimension of this region that can well accommodate only alkyl chains with less than eight carbon atoms (8). Thus, inhibitors with a longer alkyl chain should determine the accommodation of the bound moiety in the alcohol-binding site to present a more favorable conformation.

Modeling of Substrates

Kinetic investigations suggested that the substrate-induced switch observed during EST2- and M211S/R215L-catalyzed hydrolysis of long acyl chain substrates was associated to a slowing down of the acylation reaction. Unfortunately, because EST2-Hepes and M211S/R215L-HDSC are analogs of the second tetrahedral intermediate, their x-ray analysis provided us detailed structural information only on the deacylation step in the reaction mechanism. To get more insights on the acylation step of the catalytic reaction, models of the first tetrahedral intermediate were built using a simplified modeling procedure based on the EST2-Hepes and M211S/R215L-HDSC structures. This approach was justified by a large number of biological and structural studies on this class of enzymes (19), which demonstrated that first and second tetrahedral intermediates present a common acyl chain-binding pocket, oxyanion hole, tetrahedral geometrical parameters at C-1, and a nearly identical position of the catalytic triad.

*p*NP-3-[4-(2-hydroxyethyl)-piperazinyl]propionate and *p*NP-hexadecanoate esters were chosen as substrates to build the corresponding first tetrahedral intermediates with the enzymes. In both models, the carbonyl carbon of the substrate was covalently bound to the oxygen of the Ser^{155} hydroxyl group to form the tetrahedral intermediate with the proper stereochemistry and with the oxyanion directed toward the oxyanion hole formed by the backbone NH atoms of Gly^{83}, Gly^{84}, and Ala^{156}. The substrate acyl chain was modeled using as template the coordinates of the corresponding inhibitor acyl chain, whereas the alcohol moiety covalently bound to the carbonyl carbon was manually fitted in the alcohol-binding site (EST2-Hepes) or acyl-binding pocket (M211S/R215L-HDSC). All geometrical parameters were optimized on the basis of the new introduced chemical functionalities.

The generated complexes were submitted to energy minimization procedures. Because of the large number of atoms in each model, to correctly optimize the complexes the following constraints were imposed. (i) A subset centered on the ligand and comprising only the substrate and a shell of residues delimiting the alcohol- and the acyl-binding pockets was created and subjected to energy minimization. The substrate and all amino acid side chains of the shell were unconstrained during energy minimization to allow for reorientation and thus proper hydrogen bonding geometries and van der Waals contacts. (ii) All the atoms external to the subset remained fixed even if their non-bond interactions with all relaxing atoms have been calculated. The obtained models were validated by the Procheck program (18).

The analysis of the minimized models revealed a conserved orientation of the catalytic triad with all conserved H-bonds for proper catalytic machinery efficiency. Fig. 8 shows the interactions stabilized between the substrates and the enzyme binding pockets in the minimized models. It is interesting to note that in the model generated from EST2-Hepes complex, as observed in the crystal structure, the alcohol oxygen is hydrogen-bonded to the catalytic His^{282}, while in the model generated from the M211S/R215L-HDSC complex, as a result of the peculiar orientation of the acyl chain into the alcohol-binding site, this hydrogen bond is lacking.

[2] G. De Simone, L. Mandrich, V. Menchise, V. Giordano, F. Febbraio, M. Rossi, C. Pedone, and G. Manco, unpublished results.

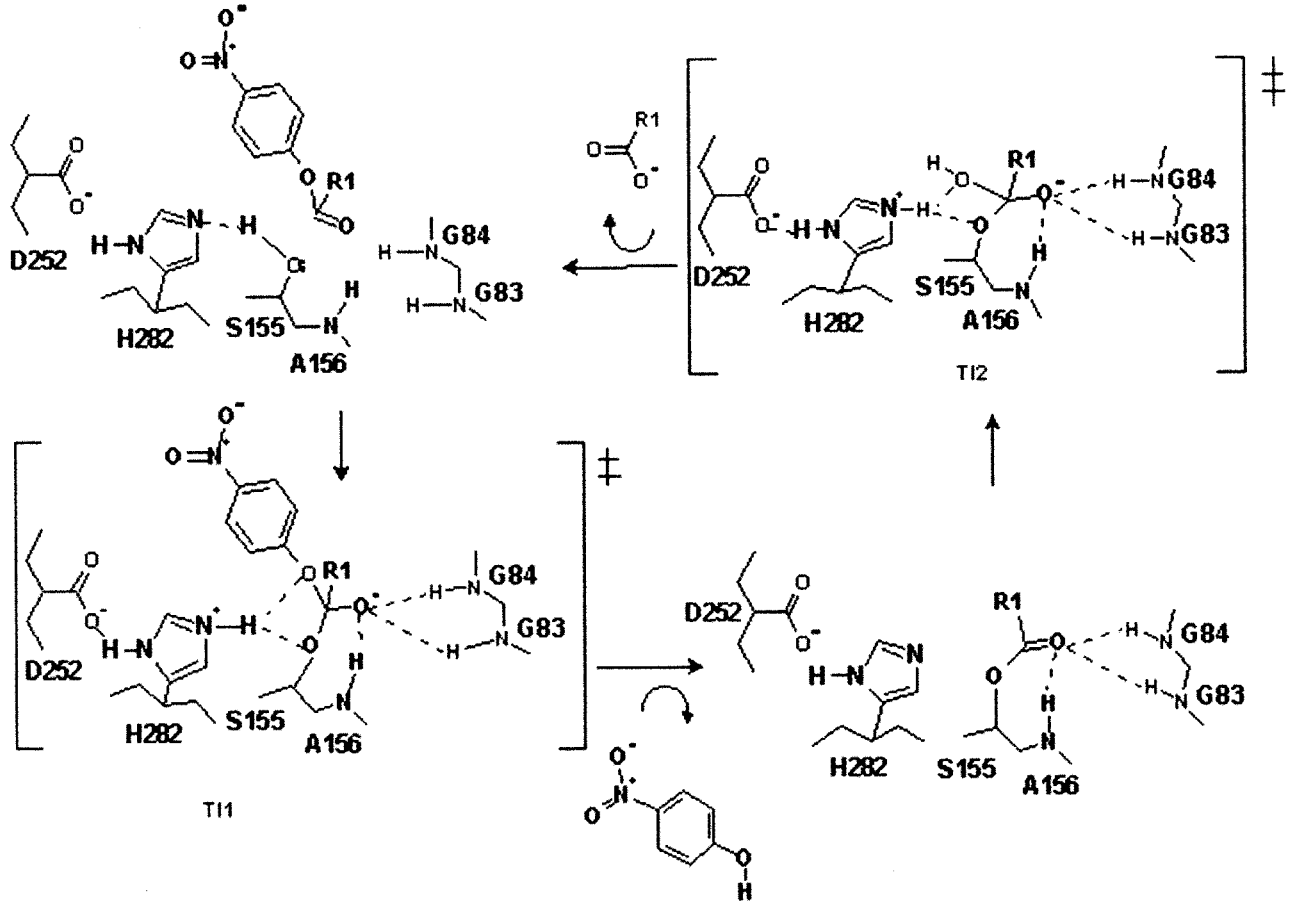

FIG. 9. **Mechanism of ester hydrolysis by EST2.** The reaction proceeds through two intermediate transition states: *TI1* and *TI2*. The hydrogen bonds have been assigned according to the EST2 wild type structure complexed with Hepes and M211S/R215L complexed with HDSC, which represent mimics of the second intermediate transition state.

DISCUSSION

In the last decade, intensified structural investigations focused on proteins belonging to the C and L groups of the carboxylesterase/lipases superfamily. In contrast, the first structural information on members of the hormone-sensitive lipase group was obtained only 4 years ago when the crystal structure of brefeldin A esterase from *Bacillus subtilis* was determined (20). Subsequently the crystal structures of EST2 from *A. acidocaldarius* (8) and AFEST from *Archaeoglobus fulgidus* (21), two novel carboxylesterase members of this family, were solved by our group as covalently bound to Hepes. Hepes was demonstrated to be a competitive inhibitor for both enzymes in aqueous solution, and its covalent adducts were formed under crystallization conditions (9). Since these adducts represented mimics of the second tetrahedral intermediate formed during the deacylation step in the catalysis, the bound Hepes molecules identified the acyl-binding pocket of both enzymes. At the same time, the structural superposition of EST2 and AFEST with *Pseudomonas cepacia* lipase complexed with a triacylglycerol analog (Protein Data Bank code 5LIP, 22) allowed the identification of the alcohol-binding pockets.

Biochemical investigation demonstrated that EST2 optimally hydrolyzes esters with acyl chain length of six or eight carbon atoms because of the small dimension of its acyl-binding pocket (6, 8). Kinetic and structural studies allowed us to propose the mechanism depicted in Fig. 9; although this mechanism refers to EST2, it should be common to all members of the hormone-sensitive lipase family. In particular, acylation of the enzyme results from the nucleophilic attack of the catalytic Ser^{155} on the ester and proceeds via formation of a tetrahedral intermediate (Fig. 9, *TI1*). Deacylation results from a nucleophilic attack of a water molecule on the acyl enzyme, again going through a tetrahedral intermediate (Fig. 9, *TI2*). Hydrogen bonds from the backbone amide groups of Ala^{156}, Gly^{83}, and Gly^{84} stabilize the negatively charged tetrahedral intermediates occurring during the catalytic reaction.

Recently mutation of residues located in the acyl-binding pocket made it possible to obtain mutated versions of EST2 with increased enzyme activity and altered specificity (9). In particular, double mutant M211S/R215L showed with *p*NP-dodecanoate a 3- and 6-fold increases of k_{cat} and s, respectively. These results were confirmed here in the absence of solvents that could interfere in the reaction mechanism by substituting water in the deacylation step. Moreover a substrate-induced change of the kinetic mechanism was also hypothesized for compounds containing long acyl chains.

In this study, a detailed analysis of all kinetic parameters involved in the multistep catalytic mechanism, together with a structural explanation of the substrate-induced switch observed for the hydrolysis of long acyl chain substrates, is provided. Kinetic measurements for wild type and double mutant enzymes using *p*NP-dodecanoate showed that the k_2 values were well below the k_3 values, thus indicating that acylation is the rate-limiting step in both cases. The higher values obtained for the activation energies E_3 with respect to E_2 were also consistent with this conclusion. Moreover the measured binding constants $k_{1,0}$ and $k_{-1,0,}$ determined for both enzyme species with *p*NP-dodecanoate suggested that for the double mutant the substrate association is faster and dissociation is slower than in the wild type enzyme (Table III). Finally the

inhibition (data not shown) exhibited by *p*NP-dodecyl ether against *p*NP-dodecanoate but not *p*NP-hexanoate esters indicate that the binding site for the short chain esters and the long chain esters are not overlapping.

Inhibition studies indicated that HDSC is a potent inhibitor for both wild type and M211S/R215L enzymes. Because the generated covalent enzyme-inhibitor complex is an analog of the second tetrahedral intermediate formed during the deacylation step (Fig. 9), HDSC was used to investigate the structural basis responsible for the switch in the mechanism and the activation observed for the double mutant with *p*NP-dodecanoate. This approach was justified on the basis of the similar behavior of this enzyme toward *p*NP-dodecanoate, *p*NP-tetradecanoate, and *p*NP-hexadecanoate substrates (9).

The structure of the M211S/R215L mutant complexed with HDSC was solved by x-ray diffraction studies. On the basis of the three-dimensional structures of other lipase/esterase complexes with alkylsulfonyl derivatives (8, 21), the hexadecane moiety of the inhibitor was expected in the well identified enzyme acyl-binding site. In contrast, our data revealed its surprising localization in the enzyme alcohol-binding pocket. The unexpected accommodation of the HDSC within this region could explain the peculiar biochemical behavior of the enzyme with respect to long acyl chain substrates. In fact, the steric hindrance of these molecules should determine the localization of their acyl chains in the alcohol-binding site and not in the acyl-binding site, thus generating the inversion of the rate-limiting step during catalysis that was observed experimentally.

To provide effective catalysis in the acylation step of the catalytic reaction, the alcohol oxygen of the ester substrate, receiving a proton from the active site histidine, must be within hydrogen bonding distance from the NE2 of this residue (see Fig. 9). In the model of the first tetrahedral intermediate generated starting from the EST2-Hepes complex, we found that the catalytic His^{282} forms a hydrogen bond with the alcohol oxygen. On the contrary, in the model generated starting from the M211S/R215L-HDSC complex, as result of the peculiar orientation of the acyl chain into the alcohol-binding site, this hydrogen bond is lacking, thus impairing the acylation step of the catalytic reaction. However, certain flexibility at high temperature, as suggested by the K_m value increase with temperature (Table II) and previous results (23), could reduce the distance between the alcohol oxygen atom and His^{282} NE2, thus allowing catalysis to occur. This phenomenon should generate the rate-limiting step inversion measured during the hydrolysis of long acyl chain substrates.

In conclusion, although the interpretation of the substrate-induced switch in the mechanism fits well with all experimental data reported, the activation observed in the double mutant is less clear. This phenomenon could depend on the interaction of the alcohol moiety sitting in the acyl-binding pocket with Met^{211} and/or Arg^{215} side chains in the wild type enzyme. This interaction could slow down the alcohol release in the wild type but not in the mutant. Support for this hypothesis comes from the consideration that for wild type the k_i with HDSC was higher than in the double mutant, meaning a faster entering of the acyl moiety. In contrast, in the wild type, substrate *p*NP-dodecanoate binds to the active site more slowly than in the double mutant (see Table IV), thus suggesting a significant role of the alcohol moiety in determining the rate of hydrolysis.

In this study, the structural reasons explaining the observed inversion in the mechanism of EST2 from *A. acidocaldarius* induced by the growing of the acyl chain in ester substrates is provided. All kinetic parameters were interpreted on the basis of an unexpected accommodation of the acyl moiety in the enzyme alcohol-binding site. There are very few cases in the literature similar to that described here. For example, something analogous has been reported to explain the enantioselectivity in some lipolytic enzymes (16) or the different substrate specificity of human cocaine esterase (24). In both cases, the switch in the binding mode was just related to a different chemoselectivity or enantioselectivity and not to the kinetic mechanism. The results reported here are interesting from both a theoretical and biotechnological point of view, and they could enable the design of mutagenic experiments for the development of more selective and efficient esterases.

Acknowledgment—We thank M. Wilmanns for giving us the opportunity to collect data at the European Molecular Biology Laboratory outstation, Hamburg, Germany.

REFERENCES

1. Hemilä, H., Koivula, T. T., and Palva, I. (1994) *Biochim. Biophys. Acta* **1210,** 249–253
2. Manco, G., Adinolfi, E., Pisani, F. M., Carratore, V., and Rossi, M. (1997) *Protein Pept. Lett.* **4,** 375–382
3. Manco, G., Adinolfi, E., Pisani, F. M., Ottolina, G., Carrea, G., and Rossi, M. (1998) *Biochem. J.* **332,** 203–212
4. Osterlund, T. (2001) *Eur. J. Biochem.* **268,** 1899–1907
5. Probst, M. R., Beer, M., Beer, D., Jeno, P., Meyer, U. A., and Gasser, R. (1994) *J. Biol. Chem.* **269,** 21650–21656
6. Manco, G., Carrea, G., Giosuè, E., Ottolina, G., Adamo, G., and Rossi, M. (2002) *Extremophiles* **6,** 325–331
7. Manco, G., Febbraio, F., Adinolfi, E., and Rossi, M. (1999) *Protein Sci.* **8,** 1789–1796
8. De Simone, G., Galdiero, S., Manco, G., Lang, D., Rossi, M., and Pedone, C. (2000) *J. Mol. Biol.* **303,** 761–771
9. Manco, G., Mandrich, L., and Rossi, M. (2001) *J. Biol. Chem.* **276,** 37482–37490
10. Leatherbarrow, R. J. (1992) *GRAFIT*, Version 3.0, Erithacus Software Ltd., Staines, UK
11. Ayala, Y. M., and Di Cera, E. (2000) *Protein Sci.* **9,** 1589–1593
12. Otwinowski, Z., and Minor, W. (1997) *Methods Enzymol.* **276,** 307–326
13. Navaza, J. (1994) *Acta Crystallogr. Sect. A* **50,** 157–163
14. Brünger, A. T., Adams, P. D., Clore, G. M., DeLano, W. L., Gros, P., Grosse-Kunstleve, R. W., Jiang, J. S, Kuszewski, J., Nilges, M., Pannu, N. S., Read, R. J., Rice, L. M., Simonson, T., and Warren, G. L. (1998) *Acta Crystallogr. Sect. D Biol. Crystallogr.* **54,** 905–921
15. Jones, T. A., Zou, J. Y., Cowan, S. W., and Kjeldgaard, M. (1991) *Acta Crystallogr. Sect. A* **47,** 110–119
16. Kazlauskas, R. J. (1994) *Trends Biotechnol.* **12,** 464–472
17. Kokotos, G., Kotsovolou, S., Constantinou-Kokotou, V., Wu, G., and Olivecrona, G. (2000) *Bioorg. Med. Chem. Lett.* **10,** 2803–2806
18. Laskowski, R. A., MacArthur, M. W., Moss, D. S., and Thornton, J. M. (1993) *J. Appl. Crystallogr.* **26,** 283–291
19. Grochulski, P., Bouthillier, F., Kazlauskas, R. J., Serreqi, A. N., Schrag, J. D., Ziomek, E., and Cygler, M. (1994) *Biochemistry* **33,** 3494–3500
20. Wei, Y., Contreras, J. A., Sheffield, P., Osterlund, T., Derewenda, U., Kneusel, R. E., Matern, U., Holm, C., and Derewenda, Z. S. (1999) *Nat. Struct. Biol.* **6,** 340–345
21. De Simone, G., Menchise, V., Manco, G., Mandrich, L., Sorrentino, N., Lang, D., Rossi, M., and Pedone, C. (2001) *J. Mol. Biol.* **314,** 507–518
22. Nardini, M., Lang, D. A., Liebeton, K., Jaeger, K. E., and Dijkstra, B. W. (2000) *J. Biol. Chem.* **275,** 31219–31225
23. D'Auria, S., Herman, P., Lakowicz, J. R., Tanfani, F., Bertoli, E., Manco, G., and Rossi, M. (2000) *Proteins* **40,** 473–481
24. Bencharit, S., Morton, C. L., Xue, Y., Potter, P. M., and Redinbo, M. R. (2003) *Nat. Struct. Biol.* **10,** 349–356

A Substrate-induced Switch in the Reaction Mechanism of a Thermophilic Esterase: KINETIC EVIDENCES AND STRUCTURAL BASIS

Giuseppina De Simone, Luigi Mandrich, Valeria Menchise, Valeria Giordano, Ferdinando Febbraio, Mosè Rossi, Carlo Pedone and Giuseppe Manco

J. Biol. Chem. 2004, 279:6815-6823.
doi: 10.1074/jbc.M307738200 originally published online November 15, 2003